Materials Research Letters

ISSN: 2166-3831 (Online) Journal homepage: www.tandfonline.com/journals/tmrl20

Anomalous twinning in body-centered cubic metals

Hai Li , Zifeng Wang , Sijing Chen , Yin Zhang , Hua Hong , Ting Zhu & Li Zhong

To cite this article: Hai Li , Zifeng Wang , Sijing Chen , Yin Zhang , Hua Hong , Ting Zhu & Li Zhong (2026) Anomalous twinning in body-centered cubic metals, Materials Research Letters, 14:9, 1181-1190, DOI: 10.1080/21663831.2026.2702011

To link to this article: https://doi.org/10.1080/21663831.2026.2702011

MATER. RES. LETT.
2026, VOL. 14, NO. 9, 1181–1190
https://doi.org/10.1080/21663831.2026.2702011

MATERIALS RESEARCH LETTERS
Taylor & Francis by informa

REPORT

Anomalous twinning in body-centered cubic metals

Hai Li[a,b*], Zifeng Wang[c*], Sijing Chen[a], Yin Zhang[d], Hua Hong[a], Ting Zhu[c] and Li Zhong[a]

[a]SEU-FEI Nano-Pico Center, Key Laboratory of MEMS of Ministry of Education, School of Integrated Circuits, Southeast University, Nanjing, People's Republic of China; [b]College of Materials Science and Engineering, Instrumental Analysis Center, Taiyuan University of Science and Technology, Taiyuan, People's Republic of China; [c]Woodruff School of Mechanical Engineering, Georgia Institute of Technology, Atlanta, GA, USA; [d]State Key Laboratory for Turbulence and Complex System, Department of Mechanics and Engineering Science, Peking University, Beijing, People's Republic of China

ABSTRACT
Anomalous shear is an unusual mode of plastic deformation in body-centered cubic (BCC) metals, traditionally associated only with dislocation slip. Here, we show it can also arise from deformation twinning. Using in situ transmission electron microscopy straining and atomistic simulations, we find twins on {112} planes at low resolved shear stresses nearly half those for the primary systems. These anomalous twins originate from screw dislocation transformations and are dominant when sheared in the anti-twinning direction. They promote dislocation emission, enable relaxation-induced detwinning, and substantially enhance deformability. Our findings establish anomalous twinning as a previously unrecognized plasticity mechanism in BCC metals.

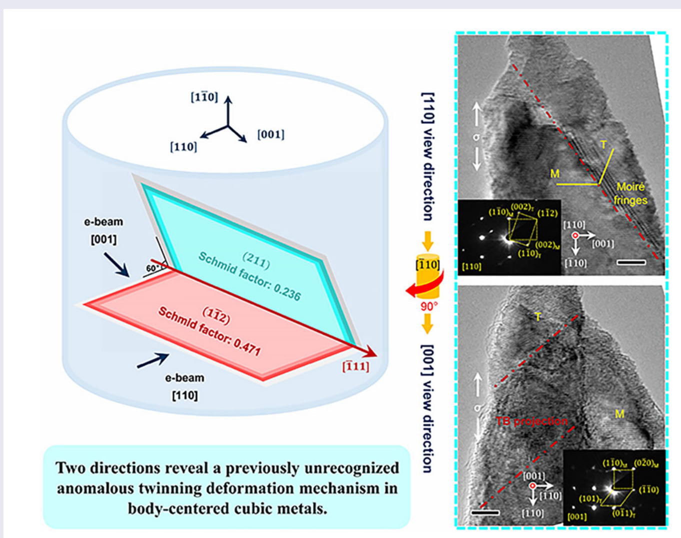

ARTICLE HISTORY
Received 21 April 2026

KEYWORDS
BCC metals; anomalous twinning; anomalous-twin-mediated dislocation plasticity; in situ TEM

1. Introduction

Anomalous shear has been studied for over fifty years in the deformation of body-centered cubic (BCC) metals [1–4]. First reported in niobium [5], it was later recognized as a common phenomenon across most BCC metals [6–9]. Anomalous shear refers to plastic deformation occurring predominantly on planes with much lower resolved shear stresses compared to the primary systems [8]. This unusual deformation mode typically involves the glide of screw dislocations at low temperatures, as high lattice resistance slows their motion [1,10–12]. It has been attributed to mechanisms such as surface-enhanced kink nucleation and elimination [9,13], and cooperative dislocation motion, either through multiple dislocations

CONTACT Ting Zhu ting.zhu@me.gatech.edu Woodruff School of Mechanical Engineering, Georgia Institute of Technology, Atlanta, GA 30332, USA; Li Zhong lizhong@seu.edu.cn SEU-FEI Nano-Pico Center, Key Laboratory of MEMS of Ministry of Education, School of Integrated Circuits, Southeast University, Nanjing 210096, People's Republic of China
*These authors contributed equally to this work.

Supplemental data for this article can be accessed online at https://doi.org/10.1080/21663831.2026.2702011.

moving together [14–17] or through multi-junction processes [1,4]. These studies have advanced our understanding of BCC metal deformation. Until now, anomalous shear has been associated only with dislocation activity. However, in BCC nanostructures, where much higher stresses can be achieved, plastic shear may shift from dislocation slip to deformation twinning, even at room temperature and low strain rates [18–20]. While such twins have been observed to form on planes with high resolved shear stresses, the possibility of twins forming on planes with low resolved shear stresses — termed *anomalous twinning* — has not been considered in BCC metals.

The deformation mode of BCC metals strongly depends on the shear direction [18,19,21,22]. When the {112} twin plane is sheared in the twinning sense, deformation twinning typically dominates plasticity [18,23–25]. In contrast, shearing in the anti-twinning sense encounters a high energy barrier for twin formation [26]. As a result, anti-twinning can only be activated under extreme conditions, such as very high applied stresses [27,28], and typically gives way to dislocation plasticity [18,29–31]. Recent experiments have shown that deformation twins in BCC metals form through 1/2 $<111>$ screw dislocations, each converting into three 1/6 $<111>$ twinning partials on adjacent {112} twin planes [19,32]. This close relationship between dislocation and twin activity, combined with the high stress levels achievable in BCC crystals that promote anomalous shear [2,9], suggests the possibility of anomalous twinning in BCC metals — a new deformation mechanism worth further exploration.

In this work, using in situ nanomechanical tests from multiple viewing directions, we clearly identify the active twinning systems and directly observe anomalous twinning in BCC metals. Under $<110>$ tension, which provides the largest resolved shear stress on the primary {112} twin plane in the anti-twinning direction, anomalous twinning becomes the dominant deformation mode on the secondary {112} twin plane in the twinning direction with low resolved shear stress. The measured twin nucleation stresses are comparable to those for dislocation activity. The anomalous twins undergo detwinning during later stages of deformation and promote dislocation emission, improving material deformability. Molecular dynamics (MD) simulations provide atomic-scale insights into the anomalous twinning and subsequent detwinning processes. These findings expand the understanding of anomalous shear mechanisms and highlight the potential of exploiting twinning-induced plasticity to enhance mechanical properties.

2. Results

2.1. Anomalous twinning in BCC crystals

To enable real-time atomic-scale observation and quantitative mechanical testing, a custom atomic force microscope (AFM) cantilever was integrated into an in situ nanomechanical testing platform (Figure 1(a), Experimental). Twinning-dominated deformation was observed during both $[\bar{1}10]$ compression (Figure 1(b)) and tension (Figure 1(c)) of W nanowires with diameters of ∼20.0 nm and ∼16.1 nm, respectively. Fast Fourier Transform (FFT) patterns (insets in Figure 1(b,c)) and magnified TEM images (Figure 1(d,e)) confirm that the atomic configurations exhibit mirror symmetry about the $(1\bar{1}2)$ plane. In BCC metals, it is well known that $[\bar{1}10]$ compression promotes twinning on the $(1\bar{1}2)$ plane due to a large resolved shear stress along the twinning direction, leading to twinning-dominated deformation in nanoscale W [18]. In contrast, $[\bar{1}10]$ tension reverses the resolved shear stress direction on the $(1\bar{1}2)$ plane, and thus promotes anti-twinning. However, because of the different atomic arrangements along the twinning and anti-twinning shear pathways, the latter faces much higher resistance and requires a higher activation stress — for example, tensile loading above 26.2 GPa [27]. Surprisingly, our quantitative measurements show the opposite trend: the twin nucleation stress under $[\bar{1}10]$ compression is approximately 1.72 times higher than under $[\bar{1}10]$ tension (Figure 1(f)). Multiple tests confirmed this behavior (Figure S3). These findings contradict the conventional anti-twinning mechanism. Furthermore, they cannot be explained by previously reported tension–compression asymmetries caused by transitions between twinning and dislocation slip [24,33] or by the effects of non-glide stresses on dislocation motion [34–37]. Therefore, our observation of twinning during $[\bar{1}10]$ tension suggests a previously unrecognized deformation mechanism.

The twin structure in Figure 1(c) is traditionally indexed as a $[\bar{1}11](1\bar{1}2)$ twin. However, because of the three-fold rotational symmetry along the $<111>$ direction in cubic structures, each $<111>$ twinning direction is shared by three {112} twin planes. For example, $[\bar{1}11]$ serves as the common twinning direction for twins on the $(1\bar{1}2)$, (211), and $(12\bar{1})$ planes. Since the (211) and $(12\bar{1})$ twin planes are equivalent under the current loading and viewing conditions, only the (211) plane is schematically shown in Figure 2(a) and considered in the following discussion. Twins on the $(1\bar{1}2)$ and (211) planes produce identical twin-matrix symmetry when viewed along the [110] direction (Figure 2(b,c)). Due to their different orientations, the $(1\bar{1}2)$ plane appears edge-on, while the (211) plane appears

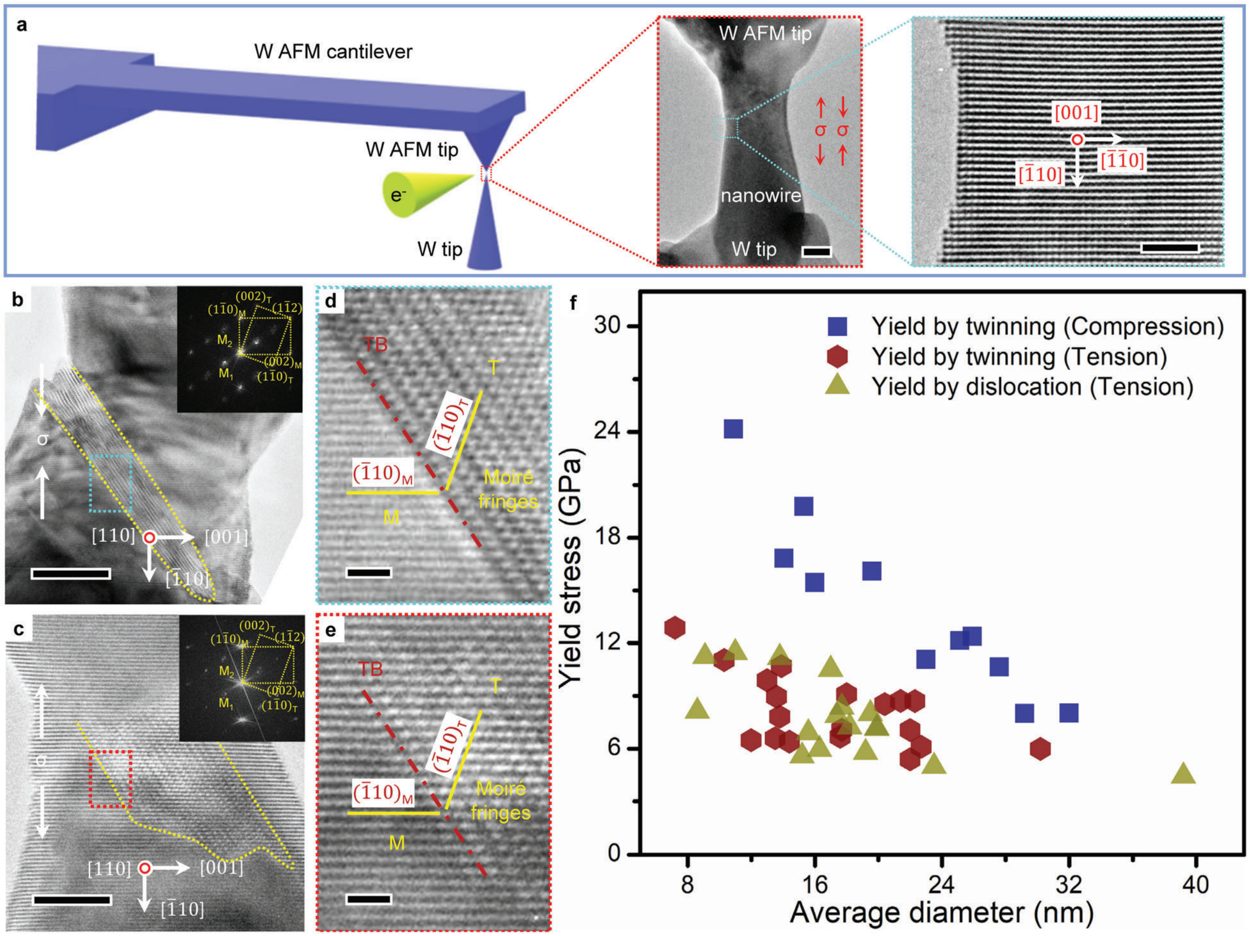

Figure 1. Twinning behavior and yield stress in [1̄10] — oriented W nanowires under compression and tension. (a) Schematic illustration of the in situ straining experiment. (b, c) Deformation twinning in [1̄10]-oriented W nanowires under compression (b) and tension (c). Twins are outlined by yellow dotted lines. Insets in (b) and (c) show the fast Fourier transform patterns of the twin. (d, e) Magnified TEM images of the dashed boxes in (b) and (c), respectively. Twin boundaries (TBs) are indicated by red dot-dash lines. Both twinned regions are filled with Moiré fringes. (f) Yield stress of W nanowires under [1̄10] compression and tension. Scale bars are 20, 2 nm (a), 5 nm (b, c), and 1 nm (d, e).

inclined when viewed along the [110] direction. When the twin boundary (TB) is parallel to the twin plane, the only difference between the [110] views of the [1̄11](11̄2) and [1̄11](211) twins appears in the projected TB region: the former shows a sharp interface (indicated by a red dotted line in Figure 2(b)), while the latter exhibits a transition region (outlined by two parallel red dotted lines in Figure 2(c)) with Moiré fringes caused by the overlap of twin and matrix lattices. However, deformation twins in BCC metals typically form multi-faceted shapes, with boundaries not perfectly parallel to the twin planes, resulting in widespread Moiré fringes across the twinned region [19,32,38,39]. This characteristic produces Moiré fringes in the [110] projection regardless of the twinning system, making it difficult to distinguish between [1̄11](11̄2) and [1̄11](211) twins based on [110] images alone. Therefore, the twin symmetry observed along [110] with abundant Moiré fringes (e.g. Figure 1 and S4) cannot unambiguously determine the specific twinning system of < 111 > {112} twins in BCC structures.

To distinguish between the [1̄11](11̄2) (Figure 2(b)) and [1̄11](211) (Figure 2(c)) twinning systems, the twin structures were rotated 90° about the loading direction to the [001] viewing direction of the matrix (Figure 2(d-g), Movies S1 and S2). The two types of twins exhibit different twin-matrix configurations, corresponding to horizontal (Figure 2(f)) and tilted TB projections (Figure 2(g)) in the simulated images. Based on this analysis, we experimentally rotated the as-formed twins about the loading direction from the [110] to the [001] viewing direction, and observed in all cases tilted TB projections under [1̄10] tension (Figure 2(h-i), and S5), while horizontal TB projections were observed under compression (Figure S6). The slight deviation of experimentally observed TB projections and simulation

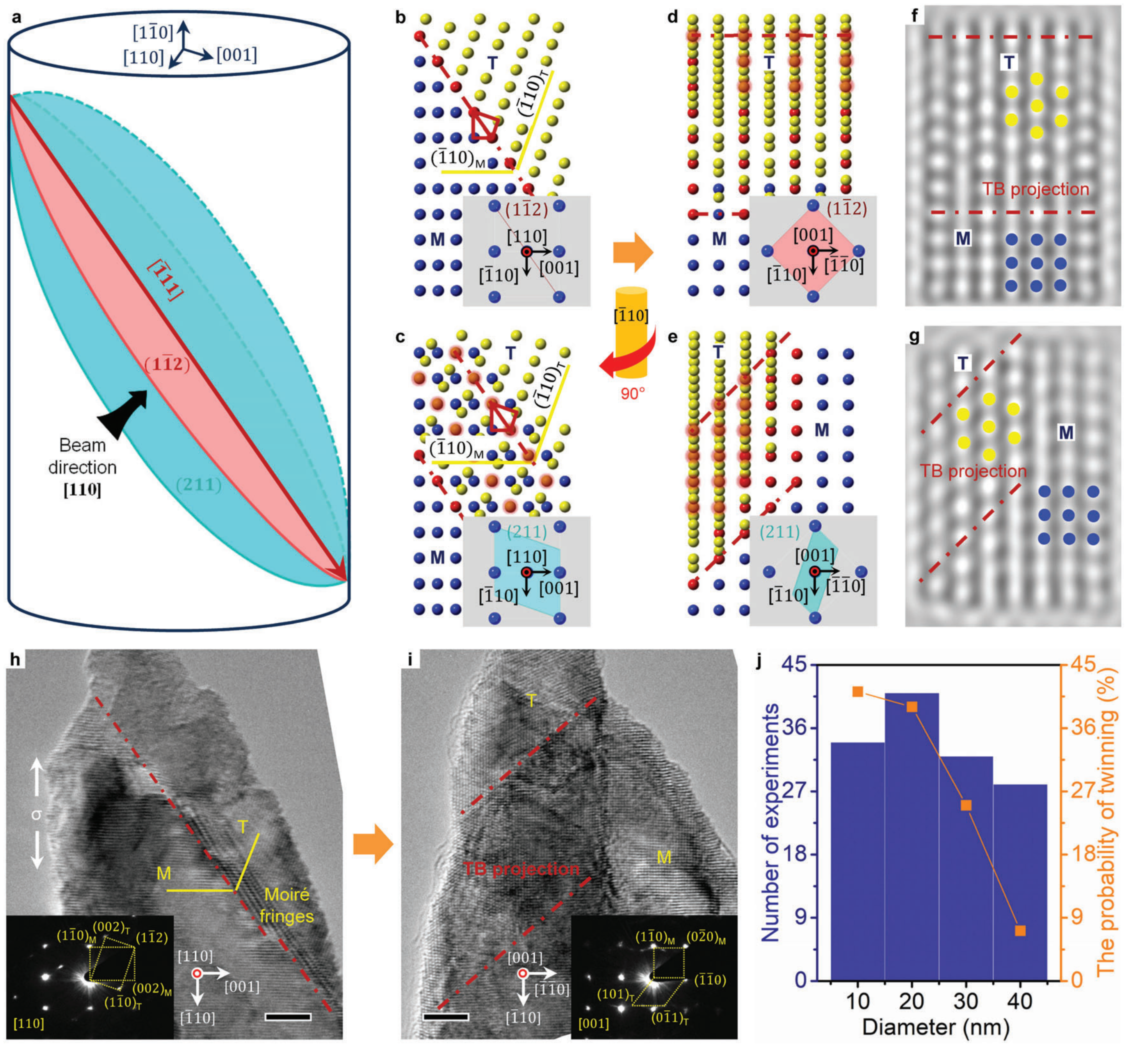

Figure 2. Anomalous twinning under $[\bar{1}10]$ tension. (a) Schematic illustration of the $[\bar{1}11](1\bar{1}2)$ and $[\bar{1}11](211)$ twinning systems under $[\bar{1}10]$ tension. (b, c) Atomic structures of the $[\bar{1}11](1\bar{1}2)$ and $[\bar{1}11](211)$ twins viewed along the [110] direction of the matrix. Both structures exhibit the same twin-matrix symmetry. Atoms in the matrix, twin, and TB are colored in blue, yellow and red, respectively. Insets in (b) and (c) schematically show [110] projections of the $(1\bar{1}2)$ and (211) planes within a unit cell, respectively. (d-g) Atomic structures (d, e) and simulated high-resolution TEM images (f, h) of the $[\bar{1}11](1\bar{1}2)$ and $[\bar{1}11](211)$ twins after a 90° rotation about the $[\bar{1}10]$ axis of the matrix (i.e. the loading direction) to a viewing direction of [001]. The $[\bar{1}11](1\bar{1}2)$ twin exhibits a horizontal TB projection (d, f), while the $[\bar{1}11](211)$ twin demonstrates a tilted TB projection (e, g). Insets in (d) and (e) show [001] projections of the $(1\bar{1}2)$ and (211) twin planes, respectively. Yellow and blue dotted patterns in (f, g) indicate the atomic arrangements in the twin and matrix. (h, i) TEM images of the same $[\bar{1}10]$ tension twin in a W nanocrystal viewed along the [110] (h) and [001] (i) directions, in good agreement with projections of the $[\bar{1}11](211)$ twin structure. Insets in (h) and (i) show the selected area electron diffraction patterns. (j) Dependence of anomalous twinning probability on the diameter of W nanocrystals. Red dot-dash lines in (b-h) indicate the direction of TB projections. Scale bars are 5 nm (h, i).

results is likely due to the TBs not being perfectly parallel to the (211) twin plane [19,39,40]. These observations unambiguously show that conventional $[1\bar{1}\bar{1}](1\bar{1}2)$ twins form under $[\bar{1}10]$ compression, while unexpected $[\bar{1}11](211)$ twins develop under $[\bar{1}10]$ tension. In addition, an edge-on twin plane can occasionally be identified in local regions of the $[\bar{1}10]$ tension TB viewed along the $[11\bar{3}]$ direction, further corroborating the presence of a $[\bar{1}11](211)$ twin structure (Figure S7). It is worth noting that the Schmid factor of the $[\bar{1}11](211)$ twinning system is only 0.236, much smaller than 0.41 for dislocation slip on the primary slip system (Table S1), thus revealing an anomalous twinning mechanism. This behavior was consistently observed in both in situ experiments and MD simulations under $[\bar{1}10]$ tension (Movies S3 and S4, Figure S8). A statistical study further shows that the probability of anomalous twinning in W nanowires under $[\bar{1}10]$ tension rapidly increases with decreasing nanowire diameter and reaches approximately 40% in the sub-20 nm regime (Figure 2(j)). As such, anomalous twinning becomes one of the major deformation modes in BCC W.

2.2. Dislocation-assisted anomalous twinning

Although the $[\bar{1}11](211)$ anomalous twin under $[\bar{1}10]$ tension experiences about half the resolved shear stress of the $[1\bar{1}\bar{1}](1\bar{1}2)$ ordinary twin under $[\bar{1}10]$ compression, its nucleation stress is significantly lower. In fact, the nucleation stress for an anomalous twin is comparable to that of dislocation nucleation under $[\bar{1}10]$ tension (Figure 1(f)), suggesting a close connection between these two deformation modes. To understand the dynamic process of anomalous twinning, MD simulations were conducted on single-crystal W nanowires (Experimental). Figure 3(a) shows a dislocation nucleating at the nanowire surface and gliding into its interior. Under a high resolved shear stress (∼ 2.8 GPa), the screw segment of the dislocation line begins to transform into a twin embryo on the (211) plane (Figure 3(b), Movie S5). Within the twin layers, this embryo grows both along and perpendicular to the $[\bar{1}11]$ direction, referred to as the length and width directions, respectively (Figure 3(c–f)). While a similar MD-observed dislocation-to-twin transition on a primary twin plane has been previously reported [41], our simulations reveal the transition on a secondary twin plane with a low Schmid factor. The dislocation-to-twin transition has been shown to involve a substantially lower energy barrier than direct surface nucleation of deformation twins [19], providing an energetically favorable pathway for anomalous twin formation in BCC structures. The inset of Figure 3(c) shows the blue-dashed $(\bar{1}11)$ cross-section of the twin embryo, revealing the formation of three twin layers bounded by coherent (211) TBs at the top and bottom. Figure 3(d,e) displays the twin thickening process, where twin partials nucleate from the nanowire surface and move inward along a (211) TB, thickening the twin embryo layer by layer. After the formation of twin partials on three consecutive layers, a curved dislocation line emits from the twin tip according to the reaction $3 \times 1/6[\bar{1}11] = 1/2[\bar{1}11]$, and continues the shearing process by gliding toward the opposite surface. The insets of Figure 3(d,e) show the $(\bar{1}11)$ cross-sections of the twin embryo with six and nine twin layers, following two sequential dislocation emissions. During the twin thickening and dislocation emission processes, a side coherent $(1\bar{1}2)$ TB forms, indicated by the red lines in Figure 3(c–e).

2.3. Detwinning under continued loading

Because of the low resolved shear stress on the anomalous twinning system and the confinement from the surrounding matrix, further twin growth is suppressed shortly after twin nucleation. The anomalous twins are unstable and undergo detwinning during continued tensile straining (Figure 4(a–d) and S9, Movie S3), resulting in a transition to dislocation-dominated deformation. Figure 4(e–h) shows the detwinning process and associated dislocation activity in the MD simulation. Figure 4(i) provides a close-up view of the atomistic detwinning process (Note S2). Detwinning leads to a gradual decrease in twin width (see the retracted red line at the twin tip in the insets of Figure 3(c–e)). This process continues until the entire twin disappears (Figure 4(i) I-III). Specifically, along the $(1\bar{1}2)$ TB at the twin tip, atoms are sheared along the detwinning direction. This shearing causes the twin to retract in the width direction, and thus detwinning occurs along the side $(1\bar{1}2)$ TB even before significant stress relaxation. This MD result aligns with the experimental observation that the twin structure struggles to grow through the nanowire (Figure 1(c)). Meanwhile, the twin continues to emit dislocations (Figure 3(c–e)), which relives stress. Since high stress is necessary to maintain the twin configuration, stress relief triggers detwinning along the (211) TB via detwinning partials $-1/6[\bar{1}11]$, causing retraction in the length direction as the expanding dislocation lines accommodate the applied strain load (Figure 4(i) IV, V, S10 and Note S2). Thus, both the twinning (Figure 3) and detwinning (Figure 4) processes are accompanied by the escape of dislocations from the surface, consistent with the experimental observations of surface step formations (insets in Figure 4(b,c)). The detwinning processes on the $(1\bar{1}2)$ (211) TBs are schematically illustrated in Figure 4(j), showing retractions along the width and length directions, respectively. Overall, the MD simulations match well with experimental observations.

3. Discussion

The above results reveal dynamic competition and cooperation between dislocation slip and anomalous twinning during deformation. Surface dislocation nucleation dominates at relatively low stresses, whereas screw dislocation segments transform into anomalous twin embryos once the applied stress exceeds a critical level. Notably, this surface nucleation mechanism remains unaffected by surface defects, which only involve changes in height and steps [19]. As anomalous twins grow and thicken, dislocations are repeatedly emitted from the twin tips, partially relaxing the local stress and destabilizing the

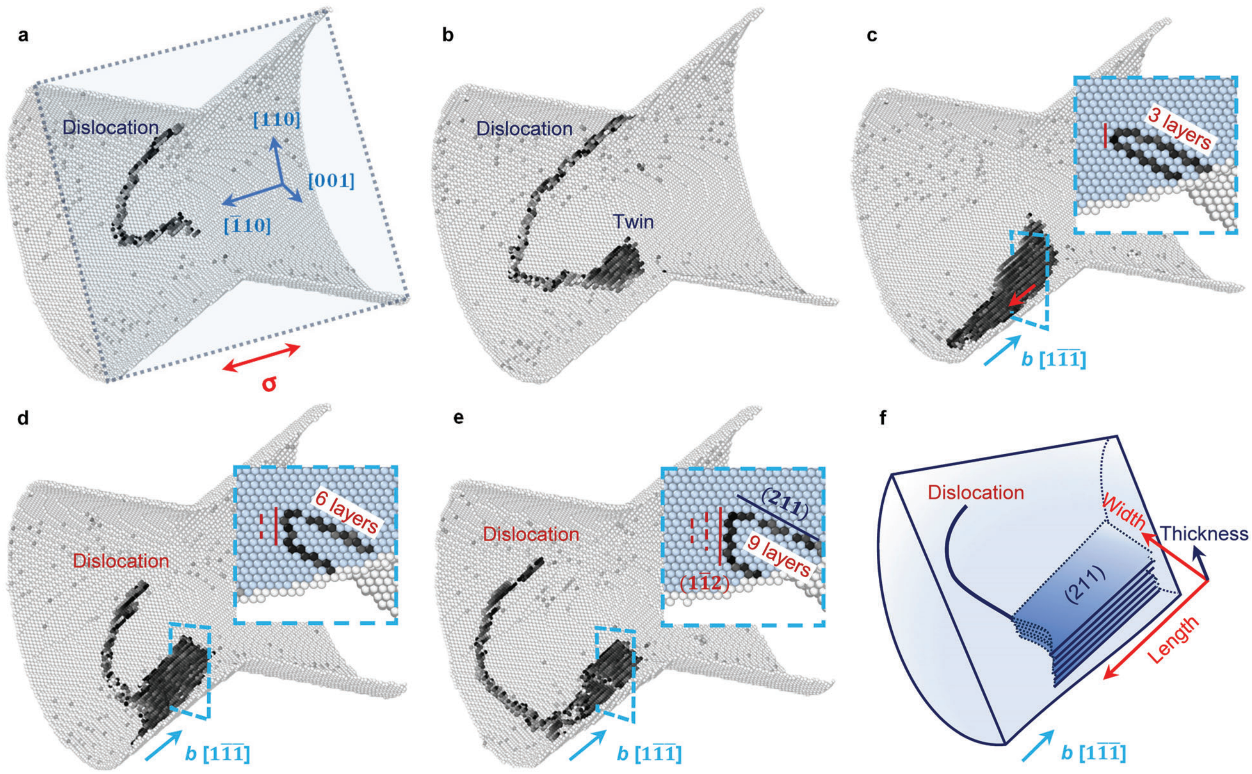

Figure 3. MD simulation of anomalous twinning behavior in a W nanowire under [$\bar{1}$10] tension. To clearly visualize the internal deformation structures, the nanowire is sectioned along the dashed plane in (a); atoms in dislocation cores and twin layers are shown in black, and surface atoms are shown in gray. (a) An edge dislocation nucleates from the surface of the nanowire and subsequently glides into the interior. (b) The screw segment of the dislocation line begins to transform into a twin embryo on the (211) plane. As the dislocation glides, it drives twin growth. (c–e) The twin thickening process and the associated dislocation activities are revealed as the twin extends along its length direction (indicated by the red arrow in c). Twin partials nucleate from the surface, causing stepwise thickening of the twin. After accumulation of three consecutive twin layers, a dislocation with a Burgers vector of 1/2[$\bar{1}$11] emits from the twin tip by reaction of three 1/6[$\bar{1}$11] twin partials, and travels toward the opposite surface. The insets in (a-c) show cross-sectional views on the blue dashed ($\bar{1}$11) plane, revealing the twin thickness evolution. Red lines mark the change in the twin tip position. (f) Schematic illustration of the twin on the (211) plane, showing its length, width and thickness directions.

twin. The subsequent detwinning process is accompanied by further dislocation activity and eventually leads to dislocation-dominated deformation. This interplay between dislocation activity and anomalous twinning-detwinning provides an effective pathway for accommodating plastic strain [42], thereby enhancing the deformability of BCC crystals.

To assess how anomalous twinning affects mechanical properties, we measured stress–strain responses during in situ straining experiments (Figure 5). As shown in Figure 5(a), a 10.7-nm-diameter W nanowire yields via anomalous twin nucleation at ~ 12 GPa (blue arrow), followed by a strain burst that causes a sudden stress drop to ~ 7 GPa. At this lower stress, the anomalous twin is unstable and undergoes spontaneous detwinning during further loading (red arrows). The detwinning process triggers dislocation activity (insets in Figure 4(b,c)), resulting in a sawtooth stress–strain curve marked by repeated stress drops. The increasing dislocation activity lowers the flow stress and accelerates complete detwinning, after which deformation becomes dislocation-dominated. This anomalous-twin-mediated dislocation plasticity improves the ductility of W nanowires. Figure 5(b) compares stress–strain curves for nanowires exhibiting anomalous twinning (blue) and those deforming via pure dislocation slip (red). Across samples of similar diameters and loading conditions, anomalous twinning consistently increases the failure strain, especially in smaller nanowires. This improvement arises from two factors: (1) anomalous twins provide additional dislocation sources beyond the surface, increasing dislocation density in otherwise dislocation-scarce nanowires and thus promoting deformability [43], and (2) detwinning removes TBs, eliminating potential fracture sites associated with stress concentration or strain incompatibility, a main failure mode in twinned BCC metals [23,44].

Anomalous twins have previously been identified in hexagonal metals as accommodation twins, which form

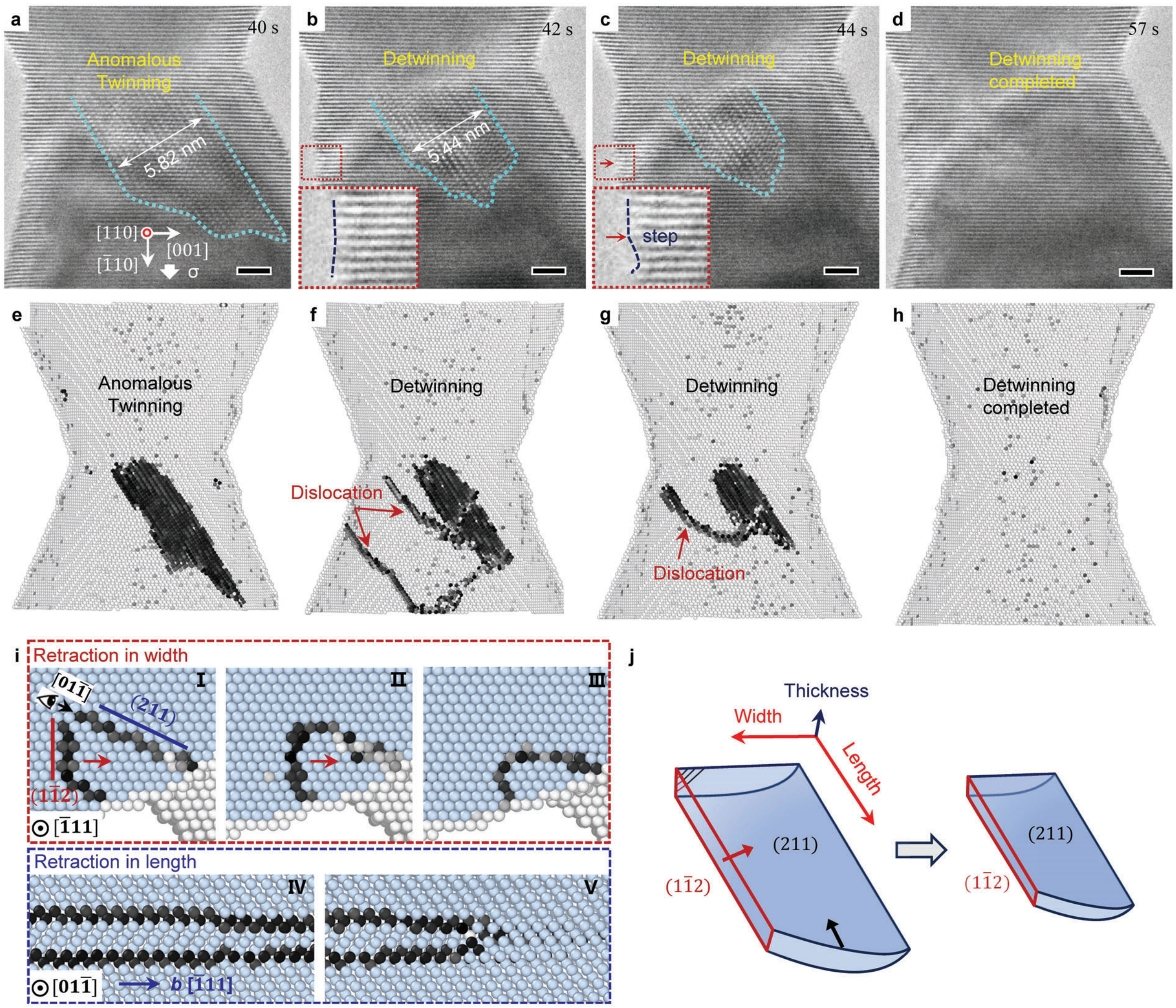

Figure 4. Detwinning process in a W nanowire under continuous loading. (a–d) Sequential TEM images showing the detwinning process in a W nanowire. The as-formed anomalous twin progressively shrinks in both the length and width directions (outlined by yellow dotted curves). Insets in (b) and (c) mark surface steps formed by dislocations escaping from the nanowire surface. (e–h) MD snapshots showing the detwinning process and the associated dislocation activity. (i) Atomic movements during detwinning in the width (I–III) and length (IV, V) directions. The viewing directions of [110] in (a–d) and [01$\bar{1}$] in i (IV, V) are parallel to the (1$\bar{1}$2) and (211) TBs, respectively, as indicated in i (I). (j) Schematics of the detwinning process. Red and blue arrows indicate the retraction of the (1$\bar{1}$2) and (211) TBs. All scale bars are 2 nm (a–d).

to relieve geometric incompatibilities between neighboring grains [45,46]. In contrast, the anomalous twins observed in this study are mechanical twins that actively contribute to deformation along the loading direction. Our analysis of plastic anisotropy reveals that the occurrence of anomalous twinning strongly depends on both the loading direction and the applied stress level. Under [$\bar{1}$10] tension, the primary twin plane (1$\bar{1}$2) has a large Schmid factor of 0.471 but is sheared in the anti-twinning sense. Many Density Functional Theory (DFT) studies [27,28,32,47–49] have consistently shown that the generalized stacking-fault energy (GSFE) barrier for anti-twinning in BCC metals is exceptionally high compared with that for ordinary twinning. In W, the resistance to anti-twinning shear is predicted to be nearly insurmountable under conventional deformation conditions [27]. In addition, our MD simulations and analysis reveal that these anomalous twins nucleate through a dislocation-to-twin transition, a pathway with a substantially lower energy barrier than direct twin nucleation. As a result, all deformation twins observed in this study are anomalous, forming through dislocation-to-twin transitions on either the (211) or (12$\bar{1}$) twin planes, which have a low Schmid factor of 0.236 (Figures 2, 3, S4 and S5). In contrast, under [$\bar{1}$10] compression, where the primary twin plane (1$\bar{1}$2) is sheared in the twinning direction, only conventional twins of the [$\bar{1}$11](1$\bar{1}$2) twin system are observed (Figure 1(a), (c) and S4). This trend persists

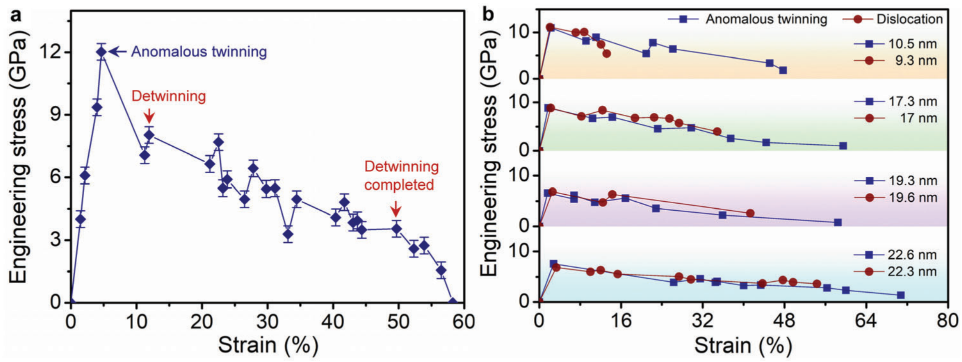

Figure 5. Impact of anomalous twinning on the mechanical properties of W nanowires. (a) Stress-strain response of a 10.7-nm-diameter nanowire exhibiting anomalous twinning. The stress rises to ∼12 GPa upon anomalous twin nucleation (indicated by a blue arrow), followed by a sharp drop to ∼7 GPa, triggering spontaneous complete detwinning (indicated by two red arrows). This twinning-detwinning process stimulates extensive dislocation activities, as indicated by repeated stress drops in the stress-strain curve. (b) Comparison of mechanical responses between deformation mediated by anomalous twinning (blue curves) and by dislocation slip (red curves). To reduce size effect, each pairwise comparison is made between nanowires of similar diameters.

under other loading orientations. For example, under $[1\bar{1}\bar{2}]$ tension, the primary twin planes $(\bar{1}21)$ and $(\bar{2}11)$, with a Schmid factor of 0.393, are also sheared in the anti-twinning sense, and deformation twins form on the $(1\bar{1}2)$, (112) and $(11\bar{2})$ planes, which have lower Schmid factors of 0.314 (Figure S11). Similar to the case of < 110 > tension, these anomalous twins detwin during further deformation, accompanied by dislocation emission, stimulating plastic deformation. MD simulations also capture anomalous twinning under < 001 > compression and < 111 > tension (Figure S12). A summary of the orientation dependence of anomalous twin formation is provided in Table S2. These findings, together with the high twinning propensity in nanoscale BCC metals, demonstrate that anomalous-twinning-mediated plasticity becomes a dominant deformation mode when primary twin planes are sheared in the anti-twinning sense. Notably, this mechanism is not unique to W but is also observed in other BCC metals such as Ta (Figure S13), indicating that anomalous twinning is a general plasticity mechanism in BCC metals.

Based on results from this study and prior work [19,32], both conventional and anomalous twinning exhibit a strong interplay with dislocation activity. Since high stress levels are known to trigger dislocation-to-twin transitions [18,19,32,50], it is plausible that similar stress conditions can also drive the transition from dislocation motion to anomalous twinning, provided that the primary twin planes are sheared in the anti-twinning direction. Indeed, in situ observations show that pre-existing dislocations in nanowires escape through the free surface during the initial stages of loading at relatively low stress levels (Figures S3 and S14). This behavior is further supported by MD simulations, which reveal that dislocations initially escape under low stresses but subsequently transform into anomalous twins once the applied stress exceeds a critical threshold (∼9.2 GPa, Figure S14), with the exact value depending on the nanowire diameter (Figure 1(f)). These results align well with previous measurements of the dislocation-to-twin transition [18,19,32]. In specimens with larger diameters, anomalous twinning is suppressed during the early and intermediate stages of deformation, when the yield and flow stresses are comparatively low. However, it becomes active in the later stages as the true stress progressively increases due to decreasing diameter, further corroborating the role of stress in anomalous twin formation (Figure S15). As a result, the observed 'smaller is stronger' trend (Figure 1f) leads to a monotonic increase in the probability for anomalous twinning with decreasing nanowire diameter (Figure 2(j)). Anomalous twinning originates from surface-nucleated dislocations that transform into twins under high stress, requiring both a free surface and sufficiently high local stress — conditions naturally satisfied in nanoscale samples. In bulk or micron-sized BCC metals, such stress levels are generally unattainable except under extreme dynamic loading [38,51]. Therefore, anomalous twinning could, in principle, be activated in bulk materials under extreme conditions. Nevertheless, because anomalous twins are unstable and tend to detwin upon stress relaxation, they may easily disappear before post–mortem characterization, making them difficult to detect in conventional ex situ experiments. The high yield and flow stresses inherent in nanoscale BCC metals thus promote anomalous twinning as a dominant deformation mechanism.

In conclusion, we uncover a previously unrecognized anomalous twinning mechanism in BCC metals, which occurs on twin planes under resolved shear stresses far lower than those required for primary slip. Originating from stress-driven dislocation transformations under high anti-twinning shear, this transient deformation mode markedly enhances deformability, offering a new pathway to overcome the strength-ductility trade-off in refractory BCC metallic materials.

Author contributions

CRediT: **Hai Li:** Conceptualization, Data curation, Formal analysis, Investigation, Methodology, Writing – original draft; **Zifeng Wang:** Formal analysis, Investigation, Resources, Software, Writing – original draft; **Sijing Chen:** Formal analysis, Funding acquisition, Investigation, Validation, Visualization; **Yin Zhang:** Formal analysis, Software, Validation, Visualization; **Hua Hong:** Formal analysis, Validation, Visualization; **Ting Zhu:** Conceptualization, Data curation, Supervision, Validation, Visualization, Writing – review & editing; **Li Zhong:** Conceptualization, Data curation, Formal analysis, Funding acquisition, Investigation, Methodology, Project administration, Supervision, Validation, Writing – review & editing

Disclosure statement

No potential conflict of interest was reported by the author(s).

Funding

L.Z. acknowledges support from the National Natural Science Foundation of China (grant number 52271142 and 92580122), the Natural Science Foundation of Jiangsu Province (grant number BK20230028), and the Fundamental Research Funds for the Central Universities. S.J.C. acknowledges support from the National Natural Science Foundation of China (grant number 52401006), the Natural Science Foundation of Jiangsu Province (grant number BK20230863), and the China Postdoctoral Science Foundation (grant number 2023M730550).

References

[1] Caillard D, Bienvenu B, Clouet E. Anomalous slip in body-centred cubic metals. Nature. 2022;609(7929):936–941. doi:10.1038/s41586-022-05087-0
[2] Srivastava K, Weygand D, Caillard D, et al. Repulsion leads to coupled dislocation motion and extended work hardening in BCC metals. Nat Commun. 2020;11:5098.
[3] Seeger A, Wasserbäch W. Anomalous slip-A feature of high-purity body-centred cubic metals. Phys Status Solidi A. 2002;189(1):27–50.
[4] Gröger R. Origin of variable propensity for anomalous slip in body-centered cubic metals. Modell Simul Mater Sci Eng. 2022;30(8):085007), doi:10.1088/1361-651X/ac9b79
[5] Duesbery MS, Foxall RA. A detailed study of the deformation of high purity niobium single crystals. Philos Mag. 1969;20(166):719–751.
[6] Wasserbäch W. Anomalous slip in high-purity niobium and tantalum single crystals. Phys Status Solidi A. 1995;147(2):417–446. doi:10.1002/pssa.2211470213
[7] Wood MI, Taylor G. Niobium-an athermal plateau in the low-temperature yield stress. Philos Mag. A. 1987;56(3):329–342. doi:10.1080/01418618708214389
[8] Hsiung LL. On the mechanism of anomalous slip in BCC metals. Mater Sci Eng A. 2010;528(1):329–337. doi:10.1016/j.msea.2010.09.017
[9] Marichal C, Srivastava K, Weygand D, et al. Origin of anomalous slip in tungsten. Phys Rev Lett. 2014;113(2):025501), doi:10.1103/PhysRevLett.113.025501
[10] Weinberger CR, Tucker GJ, Foiles SM. Peierls potential of screw dislocations in BCC transition metals: Predictions from density functional theory. Phys Rev B. 2013;87(5):054114), doi:10.1103/PhysRevB.87.054114
[11] Gröger R, Bailey AG, Vitek V. Multiscale modeling of plastic deformation of molybdenum and tungsten: I. Atomistic studies of the core structure and glide of 1/2 < 111 > screw dislocations at 0K. Acta Mater. 2008;56(19):5401–5411. doi:10.1016/j.actamat.2008.07.018
[12] Bienvenu B, Dezerald L, Rodney D, et al. Ab initio informed yield criterion across body-centered cubic transition metals. Acta Mater. 2022;236:118098), doi:10.1016/j.actamat.2022.118098
[13] Matsui H, Kimura H. Mechanism of unexpected {110} slip observed in BCC metals deformed at low-tempera tures. Scr Metall. 1973;7(9):905–913.
[14] Bulatov VV, Cai W. Nodal effects in dislocation mobility. Phys Rev Lett. 2002;89(11):115501), doi:10.1103/PhysRevLett.89.115501
[15] Bertin N, Cai W, Aubry S, et al. Enhanced mobility of dislocation network nodes and its effect on dislocation multiplication and strain hardening. Acta Mater. 2024;271:119884), doi:10.1016/j.actamat.2024.119884
[16] Yang JB, Zhang ZJ, Zhang ZF. Quantitative understanding of anomalous slip in Mo. Philos Mag. 2015;95(19):2026–2045.
[17] Zhang Z, Lu S, Yang J, et al. The criterion of anomalous slip at 0 K in body centered cubic metals. Tungsten. 2023;5(1):160–168. doi:10.1007/s42864-022-00136-7
[18] Wang J, Zeng Z, Weinberger CR, et al. Situatomic-scale observation of twinning-dominated deformation in nanoscale body-centred cubic tungsten. Nat Mater. 2015;14(6):594–600. doi:10.1038/nmat4228
[19] Zhong L, Zhang Y, Wang X, et al. Atomic-scale observation of nucleation- and growth-controlled deformation twinning in body-centered cubic nanocrystals. Nat Commun. 2024;15:560.
[20] Wei S, Wang Q, Wei H, et al. Bending-induced deformation twinning in body-centered cubic tungsten nano wires. Mater Res Lett. 2019;7(5):210–216. doi:10.1080/21663831.2019.1578833
[21] Dezerald L, Rodney D, Clouet E, et al. Plastic anisotropy and dislocation trajectory in BCC metals. Nat Commun. 2016;7:11695.
[22] Zahiri AH, Lotfpour M, Ombogo J, et al. The anisotropy of deformation twinning in BCC materials: Mechanical loading, temperature effect, and twin–twin interaction. Acta Mater. 2024;266:119681), doi:10.1016/j.actamat.2024.119681

[23] Zhao L, Chen G, Zheng H, et al. Strong size effect on deformation twin-mediated plasticity in body-centered-cubic iron. J Mater Sci Technol. 2023;144:235–242. doi:10.1016/j.jmst.2022.11.004

[24] Xiao J, Zhu L, Wang R, et al. Unveiling deformation twin nucleation and growth mechanisms in BCC transition metals and alloys. Mater Today. 2023;65:90–99. doi:10.1016/j.mattod.2023.03.028

[25] Hong Z, Kong L, Zhao X, et al. Twinning-induced shear fracture of sub-micrometer Ni-based single-crystal superalloys at 900°C. Mater Res Lett. 2025;13(8):793–800.

[26] Li X, Zhang Z, Wang J. Deformation twinning in body-centered cubic metals and alloys. Prog Mater Sci. 2023;139:101160.

[27] Wang J, Zeng Z, Wen M, et al. Anti-twinning in nanoscale tungsten, Sci Adv. 2020;6(23):eaay2792.

[28] Gröger R, Holzer J, Kruml T. Twinning and antitwinning in body-centered cubic metals. Comput Mater Sci. 2023;216:111874), doi:10.1016/j.commatsci.2022.111874

[29] Sainath G, Choudhary BK. Orientation dependent deformation behaviour of BCC iron nanowires. Comput Mater Sci. 2016;111:406–415. doi:10.1016/j.commatsci.2015.09.055

[30] Sainath G, Choudhary BK. Molecular dynamics simulations on size dependent tensile deformation behaviour of [110] oriented body centred cubic iron nanowires. Mater Sci Eng A. 2015;640:98–105. doi:10.1016/j.msea.2015.05.084

[31] Kim JY, Jang D, Greer JR. Crystallographic orientation and size dependence of tension–compression asymmetry in molybdenum nano-pillars. Int J Plast. 2012;28(1):46–52. doi:10.1016/j.ijplas.2011.05.015

[32] Wang J, Faisal AHM, Li X, et al. Discrete twinning dynamics and size-dependent dislocation-to twin transition in body-centred cubic tungsten. J Mater Sci Technol. 2022;106:33–40. doi:10.1016/j.jmst.2021.08.010

[33] Healy CJ, Ackland GJ. Molecular dynamics simulations of compression–tension asymmetry in plasticity of Fe nanopillars. Acta Mater. 2014;70:105–112. doi:10.1016/j.actamat.2014.02.021

[34] Kraych A, Clouet E, Dezerald L, et al. Non-glide effects and dislocation core fields in BCC metals. npj Comput Mater. 2019;5(1):109.

[35] Barvinschi B, Proville L, Rodney D. Quantum Peierls stress of straight and kinked dislocations and effect of non-glide stresses. Modell Simul Mater Sci Eng. 2014;22(2):025006), doi:10.1088/0965-0393/22/2/025006

[36] Clouet E, Bienvenu B, Dezerald L, et al. Screw dislocations in BCC transition metals: from ab initio modeling to yield criterion. C R Phys. 2021;22(S3):83–116. doi:10.5802/crphys.75

[37] Gröger R, Racherla V, Bassani JL, et al. Multiscale modeling of plastic deformation of molybdenum and tungsten: II. Yield criterion for single crystals based on atomistic studies of glide of $1/2 < 111 >$ screw dislocations. Acta Mater. 2008;56(19):5412–5425. doi:10.1016/j.actamat.2008.07.037

[38] Chen CQ, Florando JN, Kumar M, et al. Incipient deformation twinning in dynamically sheared BCC tantalum. Acta Mater. 2014;69:114–125. doi:10.1016/j.actamat.2014.01.046

[39] Wang X, Wang J, He Y, et al. Unstable twin in body-centered cubic tungsten nanocrystals. Nat Commun. 2020;11:2497), doi:10.1038/s41467-020-16349-8

[40] Peng H, Hou Y, Meng W, et al. Pseudo-elasticity and variable electro-conductivity mediated by size-dependent deformation twinning in molybdenum nanocrystals. Small. 2023;19(21):2206380), doi:10.1002/smll.202206380

[41] Marian J, Cai W, Bulatov VV. Dynamic transitions from smooth to rough to twinning in dislocation motion. Nat Mater. 2004;3(3):158–163.

[42] Chen G, Liu F, Tan Y, et al. Dislocation-twin-precipitate synergy imparts 2.3 GPa yield strength and 18.2% ductility in MPEA at 77 K. Mater Res. Lett. 2026;14(5):569–579.

[43] Dang C, Lin W, Meng F, et al. Enhanced tensile ductility of tungsten microwires via high-density dislocations and reduced grain boundaries. J Mater Sci Technol. 2021;95:193–202. doi:10.1016/j.jmst.2021.04.021

[44] Li L, Zhang Z, Zhang P, et al. A review on the fatigue cracking of twin boundaries: Crystallographic orientation and stacking fault energy. Prog Mater Sci. 2023;131:101011.

[45] Wu C, Lin F, Liu H, et al. Stronger and coarser-grained biodegradable zinc alloys. Nature. 2025;638(8051):684–689. doi:10.1038/s41586-024-08415-8

[46] Shi Z, Zhang Y, Wagner F, et al. On the selection of extension twin variants with low Schmid factors in a deformed Mg alloy. Acta Mater. 2015;83:17–28. doi:10.1016/j.actamat.2014.10.004

[47] Xiao J, Li S, Ma X, et al. Origin of deformation twinning in bcc tungsten and molybdenum. Phys Rev Lett. 2023;131(13). doi:10.1103/PhysRevLett.131.136101

[48] Ogata S, Li J, Yip S. Energy landscape of deformation twinning in bcc and fcc metals. Phys Rev B. 2005;71(22). doi:10.1103/PhysRevB.71.224102

[49] Wang R, Zhu L, Pattamatta S, et al. The taming of the screw: Dislocation cores in BCC metals and alloys. Mater Today. 2024;79:36–48.

[50] Zepeda Ruiz LA, Stukowski A, Oppelstrup T, et al. Probing the limits of metal plasticity with molecular dynamics simulations. Nature. 2017;550(7677):492–495. doi:10.1038/nature23472

[51] Hsiung L, Lassila D. Shock-induced deformation twinning and omega transformation in tantalum and tanta lum-tungsten alloys. Acta Mater. 2000;48(20):4851–4865. doi:10.1016/S1359-6454(00)00287-1